Design, synthesis, biological evaluations and *in silico* studies of sulfonate ester derivatives of 2-(2-benzylidenehydrazono)thiazolidin-4-one as potential α-glucosidase inhibitors ☆

Ramandeep Kaur[a], Rajnish Kumar[b], Nilambra Dogra[c], Ashok Kumar Yadav[a,*]

[a] *University Institute of Pharmaceutical Sciences, Panjab University, Chandigarh 160014, India*
[b] *Department of Neuroscience Care and Society, Division of Neurogeriatrics, Karolinska Institute, Solna 17157, Sweden*
[c] *Centre for Systems Biology & Bioinformatics, Panjab University, Chandigarh 160014, India*

ARTICLE INFO

ABSTRACT

A novel series of hydrazolyl linked sulfonate ester analogues of 4-thiazolidinone nucleus has been rationally designed, synthesized and characterized by various spectroscopic techniques including ^{1}H NMR, ^{13}C NMR and mass spectrometry. All of the synthesized derivatives were tested for *in vitro* α-glucosidase inhibitory activities and antioxidant potential. The investigated compounds displayed appreciable α-glucosidase inhibition with IC$_{50}$ values ranging from 42.80 ± 0.48 to 599.04 ± 1.26 μM in comparison to acarbose (478.07 ± 1.53 μM) and structure-activity relationship was established. Further, the safety profile of the most potent derivative (**7d**) was assessed by MTT assay in normal HEK cells. *In vivo* disaccharide loading test endorsed the higher efficacy of (**7d**) over acarbose (at a dose of 20 mg/kg of body weight) for reduction of postprandial hyperglycemia after sucrose administration. *In silico* procedures *i.e.* homology modeling, molecular docking, molecular dynamic simulations, binding free energy calculations and ADME predictive studies further justified the results of *in vitro* and *in vivo* biological investigations.

© 2021 Elsevier B.V. All rights reserved.

1. Introduction

Globally, diabetes mellitus (DM) is one of the major health concerns. The number of patients suffering from DM has been increasing sharply, and is expected to reach up to 552 million by 2030 [1]. The characteristic of this chronic disease is the hyperglycemia caused by inadequate production of insulin and/or body's inability to fully respond to insulin. An association between DM and life threatening health complications, including cardiovascular diseases, nephropathy, and retinopathy has been well established. Therefore, effective management of high blood glucose levels can prevent or delay such aligned complication [2,3]. Sulfonylureas, biguanides, meglitinides, glitazones, dipeptidyl peptidase 4 inhibitors, thiazolidinediones, sodium-glucose co-transporter inhibitors, incretin mimetic and α-glucosidase inhibitors are the major classes of clinically used antidiabetic drugs acting on different biological targets [4]. α-Glucosidase inhibitors have emerged as one of the effective therapeutic approach to manage the post-

prandial hyperglycemia, which contributes profoundly in the onset and development of DM and its associated complications [5–7]. Such inhibitors retard the intestinal glucose absorption by inhibiting the α-glucosidase which catalyzes the cleavage of 1,4-α glycosidic bonds in complex dietary carbohydrates [8]. Acarbose, miglitol, and voglibose are the examples of clinically prescribed α-glucosidase inhibitors for the treatment of T2DM. However, their extensive use has been limited by the complicated multistep procedures needed for their synthesis and undesirable side effects such as gastrointestinal intolerability, diarrhoea and flatulence [9]. Therefore, the search of new small molecules possessing potent α-glucosidase inhibitory activity and minimal side effects has recently attracted huge attention [10].

4-Thiazolidinone, a 4-carbonyl derivative of tetrahydro form of thiazole, is an ubiquitous scaffold in drug discovery as it possesses a range of exceptional pharmacological activities including antibacterial [11], antitumor [12], antihistaminic [13], anti-inflammatory [14] and anticonvulsant activity [15], anti-tubercular [16], antiviral [17]. The keto group present at the 4th position and N-C-S linkage in thiazolidinones have been accounted for its biological potential [18]. Apart from these, anti-diabetic potential of thiazolidinone heterocycle has been widely explored, which can be evi-

---

☆ Dedicated to Prof. (Dr.) Manoj Kumar. May His Soul rest in peace.
* Corresponding author.
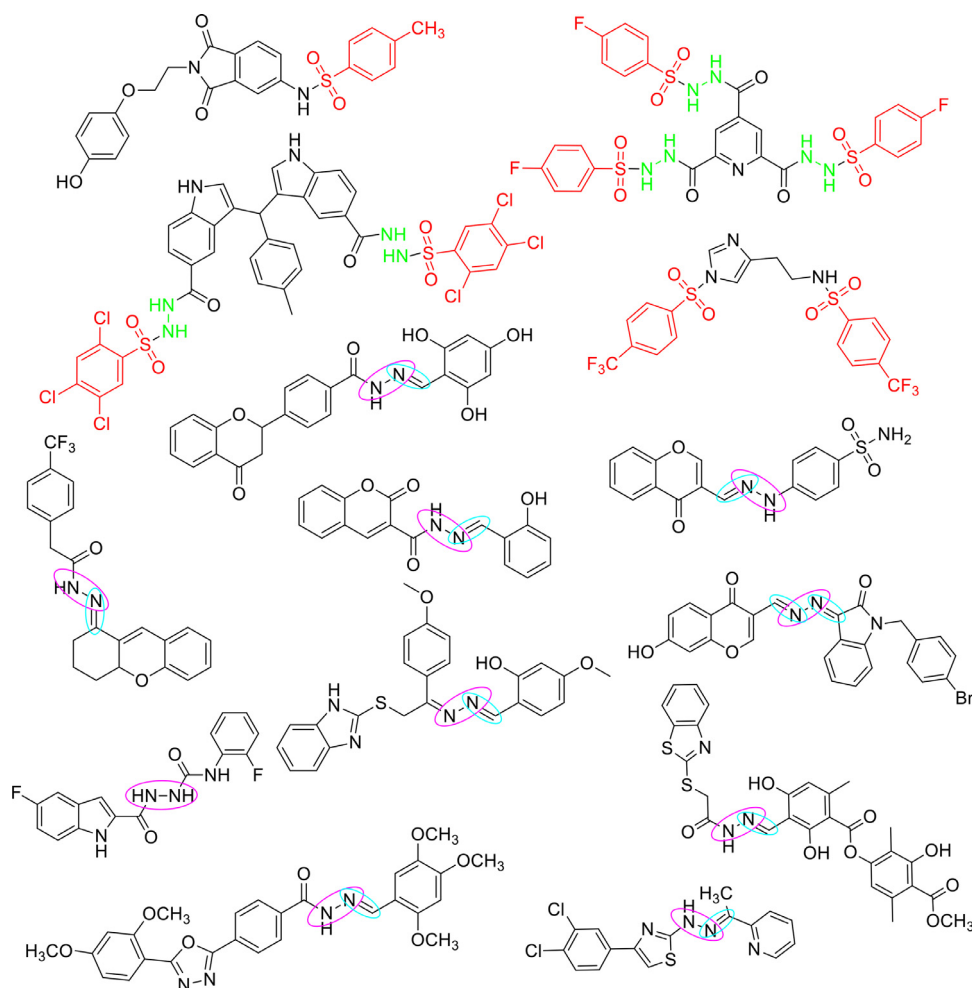 *E-mail address:* ashoky@pu.ac.in (A.K. Yadav).

Fig. 1. α-Glucosidase inhibitors containing aryl sulfonyls, imine and hydrazide scaffolds.

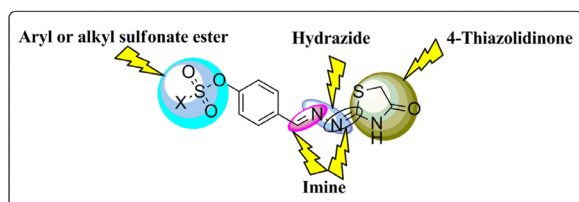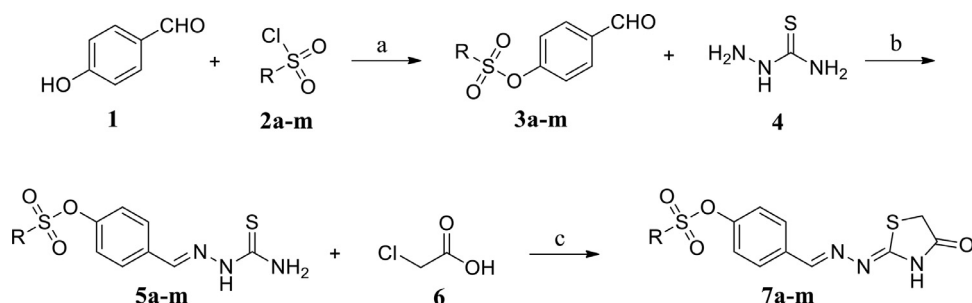**Fig. 2.** Design strategy for 4-thiazolidinone based hybrids.

[19]. These drugs act upon peroxisome proliferator activity receptor (PPARc) to exhibit their hypoglycaemic effect. Also, reports on appreciable hypoglycaemic effects produced with thiazolidinones by acting on other molecular level targets such as aldose reductase (ALR2), protein tyrosine phosphatise 1B (PTP1B), α-glucosidase and α-amylase have been published [18,20–22].

On the other hand, aryl sulfonyls are important synthons in medicinal chemistry because of their immense bioactivity [23]. They exhibit anti-inflammatory, anti-tumor and anti-fungal activities, and also inhibit HIV-1 reverse transcriptase, cyclooxygenase-2 (COX-2) [24]. Our research group has reported the PTB1B inhibitory potential of aryl sulfonyls for the management of T2DM [25]. Inhibition of α-glucosidase by aryl sulfonyls has been investigated by

denced from the successful clinical use of numerous anti-diabetic drugs *i.e.* rosiglitazone, pioglitazone, lobeglitazone and troglitazone

Scheme 1. Reagents and Conditions: (a) Dichloromethane, TEA, stir, rt, 24 h; (b) Ethanol, glacial acetic acid, 30–45 min., 50–60 °C, stir; (c) Toluene, DMF, reflux, 4-5 h.

Osella et al., and such molecules exhibited much lower IC$_{50}$ values as compared to acarbose (Fig. 1) [26–30].

It was observed from the literature that, imine (-C=N) and hydrazide (-NH-NH-) fragments are present in the number of reported α-glucosidase inhibitors (Fig. 1), which contributed considerably towards the inhibition of this enzyme [27,31–42].

Recently, we have reported the α-glucosidase inhibitory potential of thiazolidinedione–isatin [22] and pyrazole-isatin hybrids [43]. Therefore, considering the emerging importance of thiazolidinone, aryl sulfonyls, imine and hydrazide fragments, especially with regard to their α-glucosidase inhibitory properties, and as continuation of our efforts for the development of new potent α-glucosidase inhibitors, we have designed a strategy to club these four pharmacophoric units in a single molecular architecture by molecular hybridization technique in order to achieve their synergistic effect (Fig. 2).

Also, the role of oxidative stress has been well established in the pathophysiology of diabetes and associated complications [44]. Thus, the synthesized compounds were also assessed for their antioxidant properties.

2. Results and discussion

2.1. Chemistry

The title 4-thiazolidinone analogues (**7a-m**) were synthesized by three steps synthetic pathway as outlined in Scheme 1. Initially, the *O*-sulfonylation of 4-hydroxybenzaldehyde (**1**) was carried out in the presence of triethylamine (basic condition) to yield aryl/alkylsulfonate esters (**3a-m**). Further, these sulfonate esters were condensed with thiosemicarbazide (**4**) in ethanol containing catalytic amount of glacial acetic acid to get the Schiff base intermediates (**5a-m**). In the final step, Schiff base intermediates (1.0 mmol) were refluxed with chloro acetic acid (1.0 mmol) (**6**) in toluene containing small volume of DMF that resulted in the formation of 4-thiazolidinone analogues (**7a-m**). The structures of the compounds were fully characterized by ^{1}H NMR, ^{13}C NMR and Mass spectroscopic analysis. In ^{1}H NMR, a signal at δ 11.97–12.03 ppm due to –NH, and a singlet at δ 3.83–3.91 ppm due to two –CH$_2$ protons confirmed the formation of 4-thiazolidinone ring. The signal at δ 173.83–174.42 ppm in ^{13}C NMR appeared be-
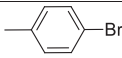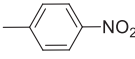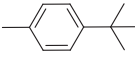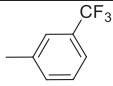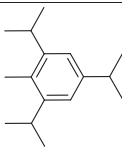
Table 1

In vitro α-glucosidase inhibitory activity and antioxidant potential of synthesized compounds.

Compound	R	α-Glucosidase inhibitory activity ± SEM (μM)	Anti-oxidant potential ± SEM (μM)
7a	—⟨⟩—CH$_3$	91.06 ± 0.69	98.78 ± 0.37
7b	—⟨⟩—Cl	253.11 ± 0.91	108.87 ± 0.91
7c	—⟨⟩	142.74 ± 0.51	103.39 ± 0.82
7d	O$_2$N-⟨⟩	42.80 ± 0.48	127.97 ± 0.42
7e	—⟨⟩—OCH$_3$	72.29 ± 0.66	94.04 ± 0.75
7f	naphthyl	198.71 ± 0.83	132.81 ± 1.01
7g	H$_3$C, H$_3$C substituted ⟨⟩—CH$_3$	56.00 ± 0.32	85.26 ± 0.84
7h	—CH$_3$	599.04 ± 1.26	223.15 ± 1.45

Table 1 (*continued*)

7i	(phenyl)—Br	291.94 ± 0.93	116.16 ± 0.52
7j	(phenyl)—NO_2	339.18 ± 1.02	131.76 ± 1.03
7k	(phenyl)—C(CH$_3$)$_3$	69.55 ± 0.72	76.95 ± 0.99
7l	(phenyl)—CF_3	182.13 ± 0.97	173.98 ± 1.12
7m	(triisopropylphenyl)	48.19 ± 0.36	62.76 ± 0.89
Acarbose	--	478.07 ± 1.53	----
Ascorbic Acid	--	---	196.51 ± 0.48

cause of the carbonyl carbon of 4-thiazolidinone. The mass spectra of compounds exhibited molecular ion peaks at $[M]^+$ and $[M+1]^+$.

2.2. In vitro α-glucosidase activity

The newly synthesized analogues (**7a-m**) showed variable degree of α-glucosidase inhibitions with IC_{50} values ranging from 42.80 ± 0.48 to 599.04 ± 1.26 μM (Table 1) in comparison with the standard drug acarbose showing an IC_{50} value of 478.07 ± 1.53 μM. Compound **7d** ($IC_{50} = 42.80 \pm 0.48$ μM) was observed to be the most potent and **7m** ($IC_{50} = 48.19 \pm 0.36$ μM) is as the second most potent derivative of the series. An interesting structure activity relationship (SAR), depicting the effect of various substituents at sulfonyl group, can be established from the results of *in vitro* enzyme inhibition assay. Different sulfonate esters affected the enzyme inhibitory activity of compounds to different extents. It is evident from the results that: (i) the arylsulfonate group appeared crucial for enzyme inhibitory activity, as a sharp decline in inhibitory activity was observed when it was replaced with alkylsulfonate (**7h**). (ii) substitution of phenylsulfonate group was preferred over naphthylsulfonate group when **7c** ($IC_{50} = 142.74 \pm 0.51$ μM) was compared with **7f** ($IC_{50} = 198.71 \pm 0.83$ μM) (iii) among the phenylsulfonate derivatives, maximum inhibitory activity (**7d**) was achieved when a hydrogen bond acceptor and electron withdrawing nitro group was present at the *ortho* position of phenyl ring, whereas, the electron withdrawing (-I) groups (Cl, Br, NO_2 and CF_3) were less influential at the *meta* and *para* positions (**7b, 7i, 7j** and **7l**, respectively) (iv) on the other hand, bulky and electron releasing (+I) groups, in case of compound **7m**, favored the inhibitory activity when present at the *ortho* and *para* positions. Concurrent substitution at the *ortho* and *para* positions appeared to be more beneficial than the mono substitution, as is in the case of **7g** ($IC_{50} = 56.00 \pm 0.32$ μM) in comparison to **7a** ($IC_{50} = 91.06 \pm 0.69$ μM). This structure activity relationship will further be well explained on the basis of molecular docking and molecular dynamic simulation studies.

2.3. Antioxidant activity

Prolonged hyperglycemia in T2DM leads to amplified generation of reactive oxygen species (ROS) and impairment of endogenous antioxidants. This oxidative stress have been implicated in the development of diabetic complications such as diabetes nephropathy, diabetes neuropathy and diabetes retinopathy [45]. Therefore, it would be beneficial if compounds possess antioxidant activity along with their α-glucosidase potential. The ferric reducing antioxidant power (PFRAP) assay was used for evaluation of reducing abilities of compounds through redox reaction with metal ions, such as iron. All compounds possessed the ability to reduce ferric ions to ferrous ions and exhibited EC_{50} values ranging from 62.76 ± 0.89 to 223.15 ± 1.45 μM. It can be visualized from the Table 1 that majority of the compounds were either more or equipotent to ascorbic acid ($EC_{50} = 196.51 \pm 0.48$ μM). Compound **7m** has been observed to be the most potent among the series with an EC_{50} value of 62.76 ± 0.89 μM. It was also observed that the substituents at phenylsulfonate moiety with +I inductive effect favored the reducing properties. The reducing ability of the synthesized compounds may serve as an indicator for their potential antioxidant efficacy that may additionally contribute towards the management of diabetic complications along with the control of post prandial hyperglycemia.

2.4. Cytotoxicity

The most potent compound (**7d**) was analyzed for its cytotoxicity in normal HEK cells by MTT assay to demonstrate its safety profile. Percent viability plot (Fig. 3) of **7d** at different assayed concentrations revealed that, more than 80% cells were viable even at
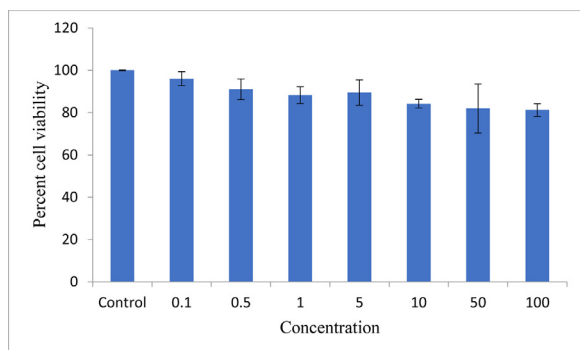
Fig. 3. Concentration versus percentage cell viability plot of 7d.

the highest tested dose (100 μM). Therefore, compound **7d** can be a candidate for further investigations.

2.5. In vivo *disaccharide loading test*

Compound **7d** was further selected for *in vivo* disaccharide loading test based upon the results of *in vitro* α-glucosidase inhibition and cytotoxicity assay. It was tested for the reduction of postprandial hyperglycemia after sucrose loading at two different doses, *i.e.*, 20 mg/kg of body weight (dose equal to standard dose of acarbose) and 10 mg/kg of body weight (half of standard dose of acarbose). The control group, administered with 0.5% CMC suspension only, exhibited a rapid increase in blood glucose concentration from 152.4 ± 4.96 to 270.6 ± 10.11 mg/dL after 30 min of sucrose administration. Subsequently, pretreatment blood glucose levels were recovered after 120 min.

The test group administered with **7d** (20 mg/kg of body weight) and acarbose (20 mg/kg of body weight) showed significant reduction in blood glucose level ($p < 0.001$, $p < 0.01$, respectively) at 30 min after sucrose loading vis-à-vis the control. However, **7d** exhibited better results than acarbose in regulating the rise of blood glucose following sucrose administration. Moreover, a decrease of 18.33 and 14.88% in area under curve (AUC) for plasma glucose was observed with **7d** and acarbose treatment, respectively from 0 to 60 min.

It was further proposed to evaluate **7d** by reducing its dose to half, *i.e.*10 mg/kg of body weight. There was no statistically significant difference observed in reduction of blood glucose concentration compared to control at 30 min after sucrose loading. However, treatment with **7d** (10 mg/kg of body weight) reduced the AUC of plasma glucose curve by 3.03% only in 60 min. It can be clearly deduced from the results that **7d** suppressed the blood glucose level in dose-dependent manner. Thus, the results of current study endorse higher efficacy of **7d** than standard drug, *viz.*, acarbose, at a dose of 20 mg/kg of body weight, in suppressing the rise of blood glucose level after sucrose administration (Fig. 4).

3. *In silico* studies

3.1. Homology model building and validation

Homology model building and validation was performed in a similar way as reported earlier [22]. Briefly, three-dimensional structure (a homology model) of α-glucosidase was developed using RaptorX server [46] taking oligo-1,6-glucosidase (PDB ID: 3A47, Gene ID: IMA1) of *Saccharomyces cerevisiae* as template structure. Validation of the homology model was performed by Ramachandran plot, Qualitative Model Energy ANalysis (QMEAN) server, Protein Structure Analysis (ProSA) tool and plot of energy as a function of amino acid sequence position. The homology model was observed to be free from artefacts and reliable to perform molecular docking and molecular dynamic simulation studies [22].

3.2. Docking studies

The most active inhibitor **7d** was selected for detailed molecular docking simulation studies to predict its interactions in bound (into the active site of α-glucosidase) conformations. Significant binding interactions including hydrogen bonding, salt bridges and hydrophobic interactions were spotted between enzyme and inhibitors. The topmost active compound (**7d**) was found to have a snug fit (docking score 5.1) inside the active site, 2D and 3D interaction has been shown in Fig. 5. 4-Thiazolidinone ring penetrated deep inside the cavity, formed from Ala 278, Arg 212, Tyr 71, Phe 177, His 348, Arg 439 including catalytic residues *i.e.* Glu 276, Asp214 and Asp 349, where it formed two hydrogen bonds with Arg 212 and Glu 276 through its oxygen and –NH, respectively. Arg 312 established two hydrogen bonds with **7d**; one with oxygen of nitro group and second with oxygen atom of sulfonyl group. Additionally, number of hydrophobic interactions along with a salt bridge between Glu 304 and nitrogen atom of nitro group further helped to stabilize the enzyme- inhibitor complex. It can be as-
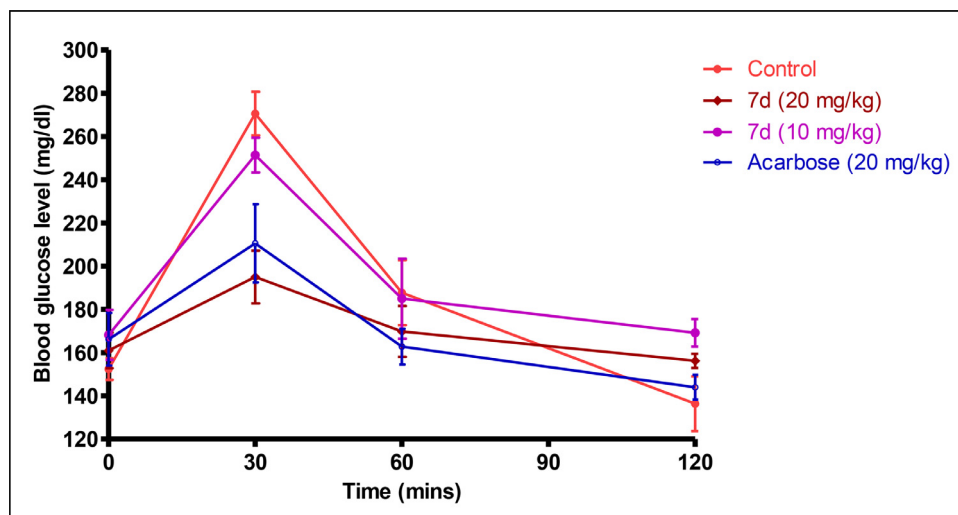

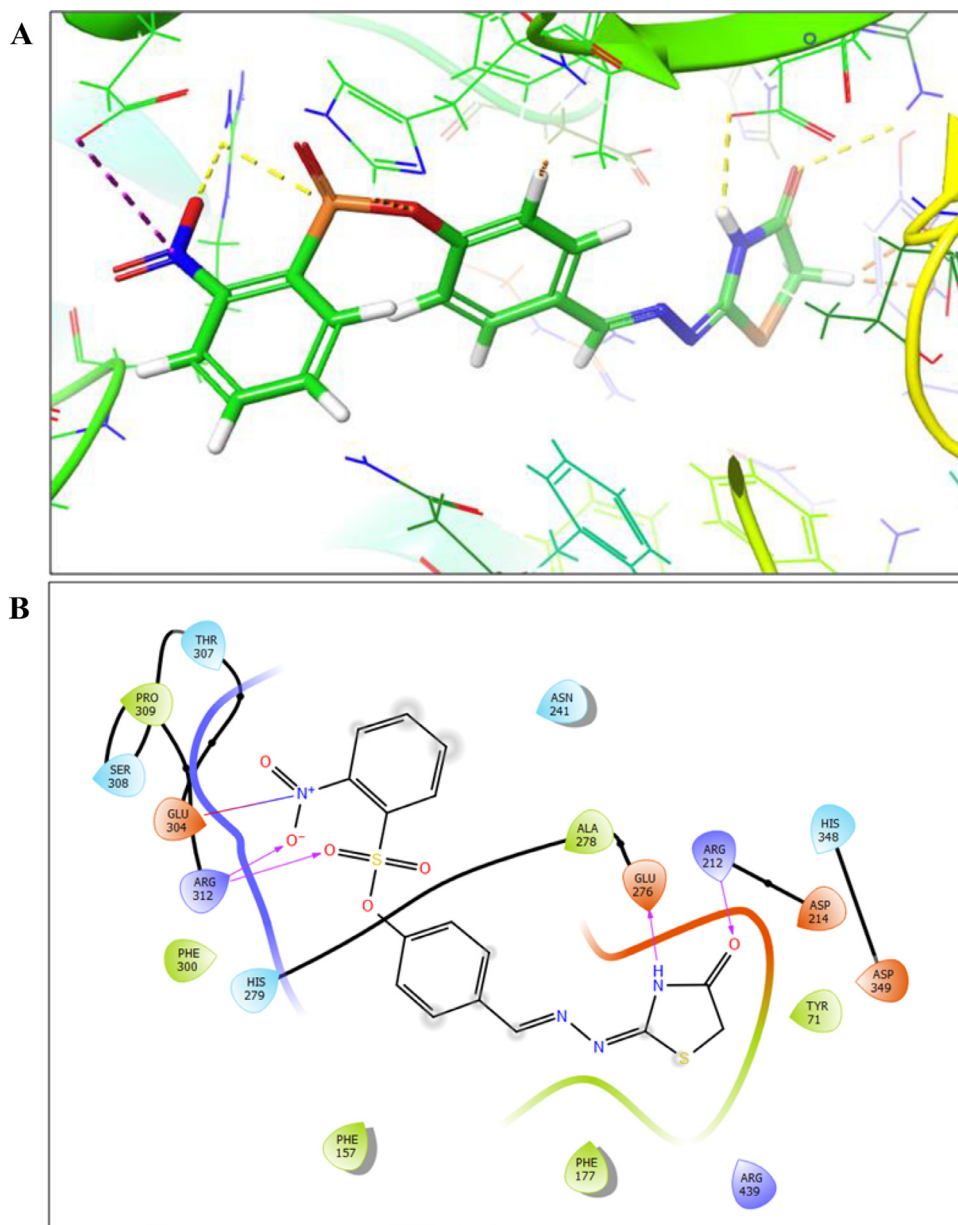**Fig. 4.** Effect of 7d and acarbose on blood glucose levels.

Fig. 5. (A) 3D binding pose of 7d, (B) 2D representation of docking interactions.

sumed that the hydrogen bonds might be the attributing reason for superior α-glucosidase inhibitory activity of **7d**.

3.3. Binding free energy calculations

The MM-GBSA method was further used to calculate the binding free energy (ΔG_{bind}) of the inhibitor enzyme complex. This method allows decomposing the total free binding energy into individual components which further facilitated the understanding of the complex binding pattern in detail *i.e.* various molecular parameters contributing in the binding of ligands and their binding mode with the enzyme. The ΔG_{bind} and other individual components participating to the binding free energy have been given in Table 2. The free energy of complexation has been observed in the range from -38.11 to -1.15 kcal/mol. The values of the binding free energy data illustrated that the Coulomb, steric van der Waals, H-bond and lipophilic interactions contributed favourably for enzyme-inhibitor complexation.

3.4. ADME predictive studies

Prediction of absorption, distribution, metabolism, excretion and toxicity (ADMET) of potential drug candidates has become an imperative part of the drug development process. It has been considered as an indispensable tool for filtration of compounds to get the molecules which are less likely to be rejected during clinical trials. Therefore, preliminary *in silico* pharmacokinetic profiling of the synthesized compounds and acarbose has been performed using QikProp v5.9 of Schrödinger suite [47]. Various physico-chemically significant and pharmaceutically relevant descriptors including QPlogPo/w, QPlogS, QPPCaco, QPlogBB, and % Human oral absorption, *etc.* for all synthesized compounds and acarbose have been presented in Table 3. The predictive ability of used methodology was validated by comparing the calculated pharmacokinetic property *i.e.* % Human oral absorption of acarbose with experimental values. The predicted value of % Human oral absorption of acarbose was found in good agreement with experi-

Table 2
Binding free energy calculations for the synthesized compounds.

Compound	ΔGbind	ΔGbind coulomb	ΔGbind Hbond	ΔGbind lipo	ΔGbind vdW	Glide Score
7a	-11.32	-12.42	-2.17	-16.25	-45.72	-3.5
7b	-38.11	-4.27	-1.36	-21.38	-41.94	-3.8
7c	-37.06	-15.68	-1.17	-16.24	-48.99	-3.9
7d	-31.28	-13.17	-1.70	-16.11	-47.13	-5.1
7e	-14.15	-16.81	-2.09	-16.81	-48.27	-4.5
7f	-35.59	-18.24	-1.17	-17.13	-52.22	-3.3
7g	-27.17	-9.90	-1.24	-17.01	-44.50	-4.4
7h	-13.80	-23.47	-2.68	-12.23	-40.02	-4.5
7i	-1.15	-6.41	-0.45	-17.36	-47.12	-2.8
7j	-17.76	-17.16	-2.42	-17.42	-50.82	-3.4
7k	-20.18	-15.64	-2.11	-19.22	-51.36	-3.5
7l	-16.71	-12.03	-0.46	-14.47	-41.78	-4.4
7m	-16.89	5.52	-0.34	-25.19	-59.07	-4.7

mentally calculated value *i.e.* 1.2% [48] and its predicted value by QikProp was 0%. The poor absorption of acarbose from gastrointestinal tract means drug stays in intestine and colon for longer period of time, thus is associated with risk of side effects such as flatulence, diarrhoea, and hypoglycaemia. Therefore, an inference may be drawn that the improved % Human oral absorption predicted for synthesized compounds may benefit in reducing their poor absorption related side effects. All other predicted parameters for synthesized compounds have also been observed within the acceptable range defined for human use, illustrating their favorable 'druggable' pharmacokinetic profile.

3.5. Molecular dynamic simulations

Conventional *in silico* docking suffer from certain limitations, majorly related to the static or semi-flexible treatment of ligands with macromolecules. During the last decade, molecular dynamics (MD) have emerged as an alternative valid tool for simulation studies. Compared to conventional docking, MD allows deep inside exploration of drug-macromolecule recognition and binding both from the mechanistic and energetic aspects. The docked complex of **7d** was subjected to molecular dynamics study to understand its atomic level interactions with the active site residues and conformation stability of ligand-enzyme complex. The Root Mean Square

Deviation (RMSD) plot of **7d** with α-glucosidase during 25 ns long MD simulation has been shown in Fig. 6**A.**

The RMSD plot indicated that the fluctuation in RMSD value were not very high, suggesting the stable nature of enzyme-inhibitor complex. Local changes along the protein chain were characterized by the Root Mean Square Fluctuation (RMSF) which gives idea about the areas of the protein that fluctuate the most over the period of simulation. RMSF trajectories plot (Fig. 6B) of enzyme indicated that most of the protein residues had RMSF values lower than 2.5 Å. Further, Ligand Root Mean Square Fluctuation (L-RMSF) was determined to get insights on ligand fluctuations *i.e.* changes in the ligand atom positions with respect to the protein. All ligand atoms exhibited the RMSF values lower than 1.5 Å expect two nitro group oxygen atoms that gave RMSF value equal to 1.5 Å (Fig. 6C).

The bar plot (Fig. 7A) showed the interaction fraction of different amino acid residues making different type of contacts with the ligand. It was observed that the hydrogen bond between Arg 312 and sulfonyl oxygen was maintained for 99%, and the hydrogen bond of carbonyl oxygen with His 348 was retained for 73% of the simulation period. It was also found that the ligand was majorly stabilized by the number of hydrophobic interactions and water bridges. The total number of specific contacts the protein makes with the **7d** over the course of the trajectory and the residue interacting with ligand in each trajectory has been given in Fig. 7**B**

Table 3
Predicted ADME parameters.

Compound	donorHB	accptHB	SASA	volume	QPpolrz	QPlogPoct	QPlogPw	QPlogPo/w	QPlogS	ClQPlogS	QPlogHERG	QPPCaco	QPlogBB	QPPMDCK	QPlogKp	QPlogKhsa	%Human Oral Absorption	Rule of Five	Rule of Three
Acarbose	17	40.6	1021.65	2055.88	58.14	67.59	64.91	-9.51	1.90	1.92	-6.05	0.006	-7.46	0.001	-11.80	-3.49	0	3	2
7a	1	9.5	703.074	1180.213	40.102	20.552	14.256	1.917	-4.765	-4.284	-6.72	163.113	-1.795	134.338	-3.348	-0.35	77.772	0	0
7b	1	9.5	693.978	1164.043	39.527	20.462	14.311	2.101	-4.922	-4.688	-6.707	162.726	-1.605	330.203	-3.324	-0.39	78.826	0	0
7c	1	9.5	669.274	1118.884	38.173	19.94	14.545	1.616	-4.193	-4.008	-6.81	165.21	-1.731	136.221	-3.144	-0.499	76.107	0	0
7d	1	10.5	700.957	1183.385	39.777	21.833	15.608	1.07	-4.196	-4.492	-6.754	37.577	-2.59	27.133	-4.421	-0.588	61.401	0	0
7e	1	10.25	707.399	1193.9	39.999	20.843	14.784	1.675	-4.387	-4.297	-6.695	159.822	-1.861	130.291	-3.273	-0.511	76.192	0	0
7f	1	9.5	715.991	1236.806	43.386	21.813	14.977	2.436	-4.984	-5.238	-7.065	182.774	-1.684	151.357	-2.876	-0.197	81.691	0	0
7g	1	9.5	726.579	1257.938	42.448	21.108	13.647	2.43	-5.162	-4.839	-6.217	240.297	-1.56	201.499	-3.303	-0.144	83.786	0	0
7h	1	9.5	587.87	949.41	30.209	16.915	13.367	0.274	-3.008	-2.453	-5.642	120.918	-1.741	96.842	-4.176	-0.863	65.822	0	0
7i	1	9.5	722.921	1199.986	41.188	21.067	14.54	2.361	-5.441	-5.576	-7.073	163.243	-1.677	356.336	-3.239	-0.309	80.376	0	0
7j	1	10.5	709.004	1193.339	39.953	21.224	15.674	0.896	-4.322	-4.492	-6.716	19.425	-2.963	13.489	-5.06	-0.566	55.249	0	1
7k	1	9.5	740.742	1306.084	43.719	21.641	13.682	2.508	-5.255	-5.119	-6.138	114.61	-1.964	93.76	-3.837	-0.057	78.484	0	0
7l	1	9.5	719.206	1216.545	41.432	21.502	14.241	2.582	-5.554	-5.357	-6.688	166.604	-1.506	607.009	-3.376	-0.258	81.826	0	0
7m	1	9.5	869.234	1574.878	52.565	24.301	12.813	4.384	-7.163	-6.533	-6.262	290.649	-1.753	247.52	-3.091	0.556	83.748	1	2

donorHB (no. of H-bond donors); **accptHB** (no. of H-bond acceptors); **SASA** (total solvent accessible surface area: $Å^2$, 300 to 1000); **Volume** (total solvent accessible volume ($Å^3$): 500 to 2000); **QPlogPoct** (Predicted octanol/gas partition coefficient: 8 to 35); **QPlogPw** (Predicted water/gas partition coefficient: 4 to 45); **QPlogPo/w** (Predicted octanol/water partition coefficient: -2.0 to 6.5); **QPlogS** (Predicted aqueous solubility: -6.5 to 0.5); **ClQPlogS** (Conformation-independent predicted aqueous solubility: -6.5 to 0.5); **QPlogHERG** (Predicted IC_{50} for blockage of HERG K^+ channels: concern < -5); **QPPCaco** (Predicted apparent Caco-2 cell, model for gut-blood barrier, permeability in nm/sec: poor if < 25 and great if > 500); **QPlogBB** (Predicted brain/blood partition coefficient: -3 to 1.2); **QPlogKhsa** (Predicted human serum albumin binding: -1.5 to 1.5); **%Human oral absorption** (high > 80% and poor < 25%); **Rule of five** (maximum 4 violations); **Rule of three** (maximum 3 violations).
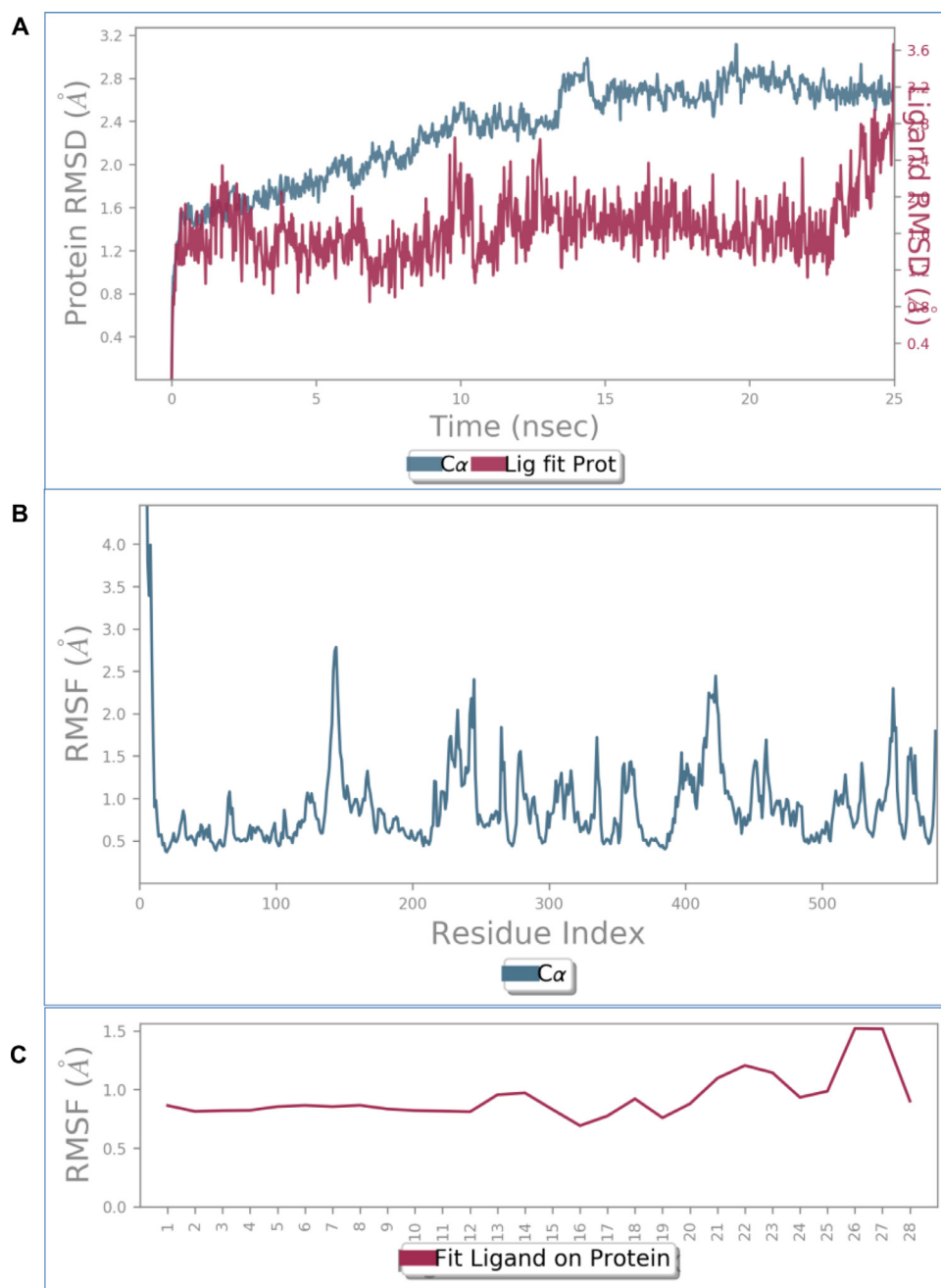
Fig. 6. (A) RMSD trajectories of α-glucosidase and 7d-α-glucosidase complex during simulation of 25 ns, (B) RMSF of α-glucosidase chain over the period of simulation (C) L-RMSF trajectories of 7d during the simulation.

and **C**. Lower values of the RMSD and RMSF, and significant number of contacts deciphered the stability of **7d** in the binding cavity of enzyme.

4. Experimental

4.1. Materials and methods

The used starting materials and solvents were purchased from the commercial sources and purified using standard procedures whenever required. Yields refer to isolated yields of products after purification. The completion of the reactions and the homogeneity of the products were monitored by thin layer chromatography (TLC) using pre-coated TLC-sheets (ALUGRAM® Xtra SIL G / UV$_{254}$).

The plates were examined under UV cabinet at 254 nm. The melting points were determined on Veego melting point apparatus and were uncorrected. The structures of the synthesized compounds were confirmed by ^{1}H NMR, ^{13}C NMR and mass spectrometry. ^{1}H and ^{13}C NMR spectra were recorded on Bruker AC-400F (400 MHz) spectrometer in deuterated dimethylsulfoxide (DMSO-d_6). The chemical shifts were reported in parts per million (ppm) using tetramethylsilane as internal standard. The spin multiplicities were indicated by the symbols: bs (broad singlet), s (singlet), d (doublet), dd (doublet of doublet), t (triplet) and m (multiplet). Mass spectrometry was conducted using Waters, Q-TOF Micromass LCT system in positive mode of electrospray ionisation (ESI-MS). All of the computational studies were carried out using Schrödinger Release 2019-1: Schrödinger, LLC, New York, NY, 2019.
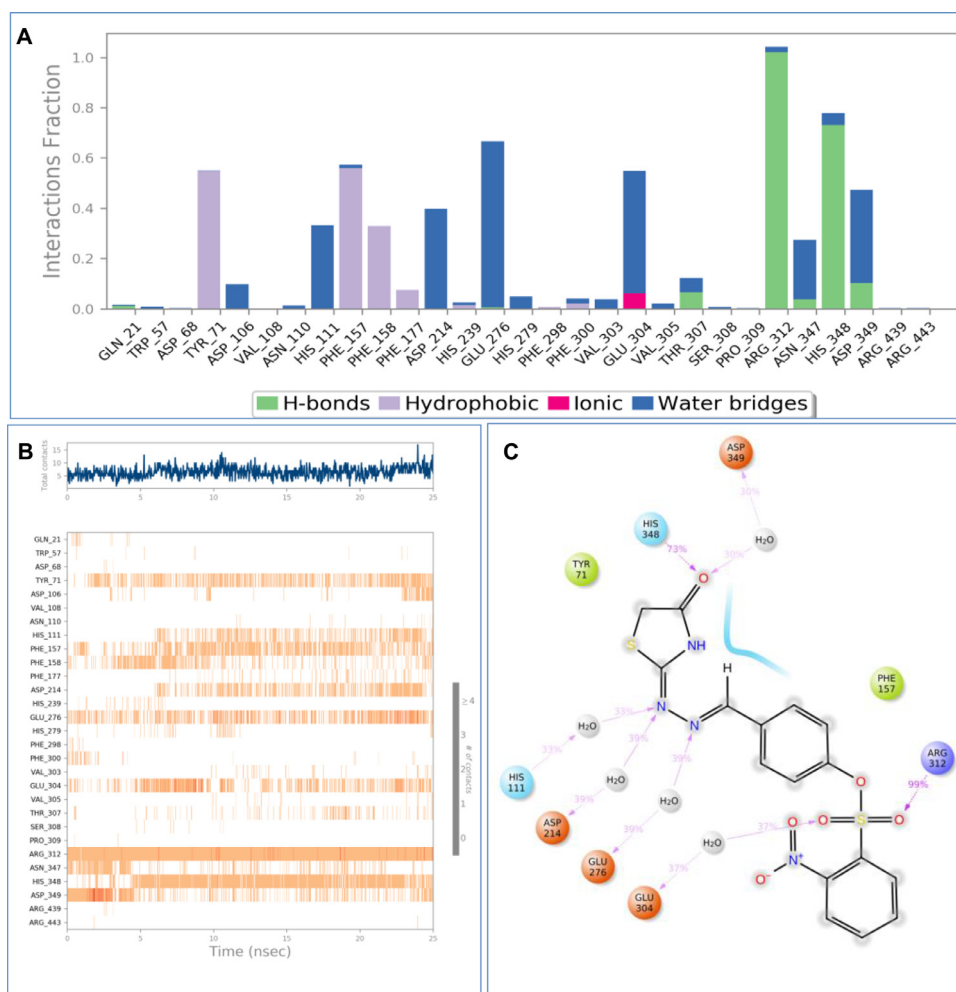
Fig. 7. (A) The bar chart of protein-ligand contacts, (B) The timeline representation of interactions and contacts. The top panel shows the total number of specific contacts the protein makes with the 7d over the course of trajectory and the bottom panel shows the residues interacting with the 7d in each trajectory frame (C) A schematic representation of detailed 7d atom interactions with the protein residues. Interactions that occurred for more than 30.0% of the simulation time in the selected trajectory (0.00 through 25.00 ns) have been shown.

4.2. General procedure for the synthesis of intermediates 3a-m

A solution of 4-hydroxybenzaldehyde (**1**) (10.0 mmol) in dichloromethane (40 mL) was stirred for 10 min. To this solution, triethylamine (11.0 mmol) was added dropwise and further stirred for 30 min. Next, various sulfonylchlorides (**2a-m**) (10.0 mmol) were added to the mixture and stirred at room temperature for 24 h. Progress of the reaction was monitored by TLC. After the completion of reaction, the reaction mixture was repeatedly washed with water and brine solution to remove the triethylamine hydrochloride salt. The organic layer was dried over sodium sulphate and solvent was removed under reduced pressure to yield intermediates **3a-m**.

4.3. General procedure for the synthesis of intermediates 5a-m

A mixture of intermediates **3a-m** (5.0 mmol) and thiosemicarbazide (5.0 mmol) were mixed in absolute ethanol (25 mL) along with few drops of glacial acetic acid. The resulting reaction mixture was stirred at 50–60 °C for 30–45 min. Progress of the reaction was monitored by TLC. After the completion of reaction, the reaction mixture was allowed to stand for half an hour, and after which a solid was separated. The solid, thus, obtained was filtered under vacuum, washed with water and dried to yield pure intermediates **5a-m**.

4.4. General procedure for preparation of compounds 7a-m

Intermediates **5a-m** (3.0 mmol) and chloroacetic acid (3.0 mmol) were added in toluene (20 mL) containing a small amount (2.0 mL) of dimethylformamide (DMF). The solution was refluxed using Dean-Stark apparatus for 4-5 h on oil bath. Progress of the reaction was monitored by TLC. After the completion of reaction, toluene was recovered under reduced pressure and the remaining concentrate was poured into ice cold water. A white colored solid was separated, which was washed with water, dried and recrystallized from methanol to obtain pure final products (**7a-m**) [49].

4.5. 4-(((4-Oxothiazolidin-2-ylidene)hydrazono)methyl)phenyl-4-methylbenzene-sulfonate (7a)

Yield: 79%; mp: 238–240 °C. ^{1}H NMR (400 MHz, DMSO-*d6*): δ 11.97 (s, 1H, N*H*), 8.33 (s, 1H, C*H*=N), 7.72–7.70 (m, 4H, Ar-*H*), 7.43 (d, 2H, *J* = 8.16 Hz, Ar-*H*), 7.04 (d, 2H, *J* = 8.68 Hz, Ar-*H*), 3.83 (s, 2H, -C*H*$_2$), 2.45 (s, 3H, C*H*$_3$) ppm. ^{13}C NMR (100 MHz, DMSO-*d6*): δ 174.21 (*C*4-thiazolidinone ring), 164.82 (*C*2-thiazolidinone ring), 154.81 (H*C*=N), 150.28, 145.95, 133.29, 131.18, 130.27, 129.13, 128.23, 122.56 (Aromatic *C*), 33.00 (*C*5-thiazolidinone ring), 21.15 (*C*H$_3$) ppm. Mass (ES$^+$): 390.1596 (M+1)$^+$.

4.6. 4-(((4-Oxothiazolidin-2-ylidene)hydrazono)methyl)phenyl-4-chlorobenzenesulfonate (7b)

Yield: 78%; mp: 243–245 °C. ^{1}H NMR (400 MHz, DMSO-*d6*): δ 11.99 (s, 1H, N*H*), 8.35 (s, 1H, C*H*=N), 7.87–7.84 (m, 2H, Ar-*H*), 7.76–7.73 (m, 2H, Ar-*H*), 7.71–7.68 (m, 2H, Ar-*H*), 7.12–7.08 (m, 2H, Ar-*H*), 3.85 (s, 2H, C*H$_2$*) ppm. ^{13}C NMR (100 MHz, DMSO-*d6*): δ 174.42 (*C*4-thiazolidinone ring), 165.01 (*C*2-thiazolidinone ring), 154.78 (H*C*=N), 150.07, 140.22, 133.53, 132.86, 130.17, 130.06, 129.24, 122.63 (Aromatic *C*), 33.00 (*C*5-thiazolidinone ring) ppm. Mass (ES$^+$): 411.0873 (M+1)$^+$.

4.7. 4-(((4-Oxothiazolidin-2-ylidene)hydrazono)methyl)phenyl benzenesulfonate (7c)

Yield: 76%; mp: 247–248 °C. ^{1}H NMR (400 MHz, DMSO-*d6*): δ 12.02 (s, 1H, N*H*), 8.38 (s, 1H, C*H*=N), 7.89–7.87 (m, 2H, Ar-*H*), 7.85–7.82 (m, 1H, Ar-*H*), 7.75 (d, *J* = 8.76 Hz, 2H, Ar-*H*), 7.70–7.67 (m, 2H, Ar-*H*), 7.27 (d, *J* = 8.72 Hz, 2H, Ar-*H*), 3.91 (s, 2H, C*H$_2$*) ppm. ^{13}C NMR (100 MHz, DMSO-*d6*): δ 174.17 (*C*4-thiazolidinone ring), 164.81 (*C*2-thiazolidinone ring), 154.80 (H*C*=N), 150.21, 135.16, 134.08, 133.37, 129.86, 129.15, 128.20, 122.56 (Aromatic *C*), 32.99 (*C*5-thiazolidinone ring) ppm. Mass (ES$^+$): 376.1496 (M+1)$^+$.

4.8. 4-(((4-Oxothiazolidin-2-ylidene)hydrazono)methyl)phenyl-2-nitrobenzenesulfonate (7d)

Yield: 80%; mp: 255–257 °C. ^{1}H NMR (400 MHz, DMSO-*d6*): δ 12.03 (s, 1H, N*H*), 8.41 (s, 1H, C*H*=N), 8.22 (dd, *J* = 8.0 Hz, 1.0 Hz, 1H, Ar-*H*), 8.10–8.06 (m, 1H, Ar-*H*), 8.02–7.99 (m, 1H, Ar-*H*), 7.91–7.87 (m, 1H, Ar-*H*), 7.82–7.79 (m, 2H, Ar-*H*), 7.28–7.25 (m, 2H, Ar-*H*), 3.90 (s, 2H, C*H$_2$*) ppm. ^{13}C NMR (100 MHz, DMSO-*d6*): δ 174.09 (*C*4-thiazolidinone ring), 164.82 (*C*2-thiazolidinone ring), 154.71 (H*C*=N), 149.83, 147.91, 137.16, 133.89, 133.11, 131.81, 129.41, 125.91, 125.44, 122.48 (Aromatic *C*), 33.01 (*C*5-thiazolidinone ring) ppm
Mass (ES$^+$): 420.9240 (M)$^+$, 421.9440 (M+1)$^+$.

4.9. 4-(((4-Oxothiazolidin-2-ylidene)hydrazono)methyl)phenyl-4-methoxybenzenesulfonate (7e)

Yield: 76%; mp: 260–261 °C. ^{1}H NMR (400 MHz, DMSO-*d6*): δ 12.01 (s, 1H, N*H*), 8.38 (s, 1H, C*H*=N), 7.81–7.78 (m, 2H, Ar-*H*), 7.77–7.73 (m, 2H, Ar-*H*), 7.18–7.15 (m, 2H, Ar-*H*), 7.13–7.09 (m, 2H, Ar-*H*), 3.90 (s, 2H, C*H$_2$*), 3.86 (s, 3H, OC*H$_3$*) ppm. ^{13}C NMR (100 MHz, DMSO-*d6*): δ 174.07 (*C*4-thiazolidinone ring), 164.82 (*C*2-thiazolidinone ring), 154.86 (H*C*=N), 164.08, 150.35, 133.23, 130.65, 129.12, 125.24, 122.62, 114.98 (Aromatic *C*), 55.91 (OC*H$_3$*), 33.00 (*C*5-thiazolidinone ring) ppm. Mass (ES$^+$): 405.9191 (M)$^+$, 406.9012 (M+1)$^+$.

4.10. 4-(((4-Oxothiazolidin-2-ylidene)hydrazono)methyl)phenyl naphthalene-2-sulfonate (7f)

Yield: 80%; mp: 248–250 °C. ^{1}H NMR (400 MHz, DMSO-*d6*): δ 12.00 (s, 1H, N*H*), 8.62–8.61 (m, 1H, Ar-*H*), 8.35 (s, 1H, C*H*=N), 8.23 (d, 2H, *J* = 9.0 Hz, Ar-*H*), 8.12 (d, 1H, *J* = 8.0 Hz, Ar-*H*), 7.89 (dd, 1H, J_1 = 8.5 Hz, J_2 = 2.0 Hz, Ar-*H*), 7.81–7.78 (m, 1H, Ar-*H*), 7.73–7.70 (m, 3H, Ar-*H*), 7.16–7.14 (m, 2H, Ar-*H*), 3.89 (s, 2H, C*H$_2$*) ppm. ^{13}C NMR (100 MHz, DMSO-*d6*): δ 173.99 (*C*4-thiazolidinone ring), 164.84 (*C*2-thiazolidinone ring), 154.72 (H*C*=N), 150.19, 135.01, 133.28, 131.34, 131.06, 130.25, 129.99, 129.96, 129.57, 129.08, 128.02, 127.91, 122.52, 122.36 (Aromatic *C*), 32.89 (*C*5-thiazolidinone ring) ppm. Mass (ES$^+$): 425.9560 (M)$^+$, 426.9821 (M+1)$^+$.

4.11. 4-(((4-Oxothiazolidin-2-ylidene)hydrazono)methyl)phenyl-2,4,6-trimethyl benzenesulfonate (7g)

Yield: 77%; mp: 242–244 °C. ^{1}H NMR (400 MHz, DMSO-*d6*): δ 12.00 (s, 1H, N*H*), 8.37 (s, 1H, C*H*=N), 7.76–7.72 (m, 2H, Ar-*H*), 7.15 (s, 2H, Ar-*H*), 7.10–7.07 (m, 2H, Ar-*H*), 3.90 (s, 2H, C*H$_2$*), 2.48 (s, 6H, C*H$_3$*), 2.30 (s, 3H, C*H$_3$*) ppm. ^{13}C NMR (400 MHz, DMSO-*d6*): δ 174.05 (*C*4-thiazolidinone ring), 164.83 (*C*2-thiazolidinone ring), 154.85 (H*C*=N), 150.10, 144.39, 139.75, 133.21, 131.87, 129.38, 129.11, 122.34 (Aromatic *C*), 32.99 (*C*5-thiazolidinone ring), 22.11 (C*H$_3$*), 20.57 (C*H$_3$*) ppm. Mass (ES$^+$): 417.9610 (M)$^+$, 418.9575 (M+1)$^+$.

4.12. 4-(((4-Oxothiazolidin-2-ylidene)hydrazono)methyl)phenyl methanesulfonate (7h)

Yield: 80%; mp: 225–227 °C. ^{1}H NMR (400 MHz, DMSO-*d6*): δ 12.01 (s, 1H, N*H*), 8.39 (s, 1H, C*H*=N), 7.77–7.73 (m, 2H, Ar-*H*), 7.16–7.12 (m, 2H, Ar-*H*), 3.90 (s, 2H, C*H$_2$*), 3.61 (s, 3H, C*H$_3$*) ppm. ^{13}C NMR (100 MHz, DMSO-*d6*): δ 174.06 (*C*4-thiazolidinone ring), 164.84 (*C*2-thiazolidinone ring), 154.78 (H*C*=N), 151.11, 130.11, 129.42, 122.54 (Aromatic *C*), 38.32 (C*H$_3$*), 32.98 (*C*5-thiazolidinone ring) ppm. Mass (ES$^+$): 313.7012 (M)$^+$, 314.7013 (M+1)$^+$.

4.13. 4-(((4-Oxothiazolidin-2-ylidene)hydrazono)methyl)phenyl-4-bromo benzenesulfonate (7i)

Yield: 84%; mp: 232–233 °C. ^{1}H NMR (400 MHz, DMSO-*d6*): δ 12.01 (s, 1H, N*H*), 8.48–8.44 (m, 2H, Ar-*H*), 8.39 (s, 1H, C*H*=N), 8.18–8.15 (m, 2H, Ar-*H*), 7.79–7.75 (m, 2H, Ar-*H*), 7.19–7.16 (m, 2H, Ar-*H*), 3.90 (s, 2H, C*H$_2$*) ppm. ^{13}C NMR (100 MHz, DMSO-*d6*): δ 174.09 (*C*4-thiazolidinone ring), 164.87 (*C*2-thiazolidinone ring), 154.72 (H*C*=N), 151.10, 149.89, 139.25, 133.74, 130.04, 129.32, 125.05, 122.63 (Aromatic *C*), 33.00 (*C*5-thiazolidinone ring) ppm. Mass (ES$^+$): 455.8911 (M+1)$^+$, 456.9318 (M+2)$^+$.

4.14. 4-(((4-Oxothiazolidin-2-ylidene)hydrazono)methyl)phenyl-4-nitrobenzenesulfonate (7j)

Yield: 80%; mp: 263–265 °C. ^{1}H NMR (400 MHz, DMSO-*d6*): δ 12.02 (s, 1H, N*H*), 8.39 (s, 1H, C*H*=N), 7.91–7.88 (m, 2H, Ar-*H*), 7.81–7.79 (m, 2H, Ar-*H*), 7.78–7.75 (m, 2H, Ar-*H*), 7.17–7.14 (m, 2H, Ar-*H*), 3.90 (s, 2H, C*H$_2$*) ppm. ^{13}C NMR (100 MHz, DMSO-*d6*): δ 174.08 (*C*4-thiazolidinone ring), 165.97 (Aromatic *C*), 164.84 (*C*2-thiazolidinone ring), 154.77 (H*C*=N), 150.07, 133.53, 133.30, 130.13, 129.41, 129.24, 122.62 (Aromatic *C*), 33.01 (*C*5-thiazolidinone ring) ppm. Mass (ES$^+$): 420.9640 (M)$^+$, 421.9740 (M+1)$^+$.

4.15. 4-(((4-Oxothiazolidin-2-ylidene)hydrazono)methyl)phenyl-4-(tert-butyl) benzenesulfonate (7k)

Yield: 73%; mp: 281–283 °C. ^{1}H NMR (400 MHz, DMSO-*d6*): δ 12.00 (s, 1H, N*H*), 8.39 (s, 1H, C*H*=N), 7.83–7.80 (m, 2H, Ar-*H*), 7.78–7.74 (m, 2H, Ar-*H*), 7.71–7.68 (m, 2H, Ar-*H*), 7.16–7.13 (m, 2H, Ar-*H*), 3.90 (s, 2H, C*H$_2$*), 1.31 (s, 9H, C*H$_3$*) ppm. ^{13}C NMR (100 MHz, DMSO-*d6*): δ 174.11 (*C*4-thiazolidinone ring), 164.87 (*C*2-thiazolidinone ring), 158.39 (Aromatic *C*), 154.82 (H*C*=N), 150.27, 133.29, 131.43, 129.14, 128.09, 126.70, 122.50 (Aromatic *C*), 35.13 (*C*(CH$_3$)$_3$), 33.00 (*C*5-thiazolidinone ring), 30.59 (C*H$_3$*) ppm. Mass (ES$^+$): 431.9892 (M)$^+$, 432.9820 (M+1)$^+$.

4.16. 4-(((4-Oxothiazolidin-2-ylidene)hydrazono)methyl)phenyl-3'-(trifluoromethyl) benzenesulfonate (7l)

Yield: 76%; mp: 236–237 °C. ^{1}H NMR (500 MHz, DMSO-*d6*): δ 12.01 (s, 1H, N*H*), 8.39 (s, 1H, C*H*=N), 8.25 (d, 1H, *J* = 8.0 Hz,

Ar-*H*), 8.21 (d, 1H, *J* = 8.0 Hz, Ar-*H*), 8.12 (s, 1H, Ar-*H*), 7.95 (t, 1H, *J* = 8 Hz, Ar-*H*), 7.79–7.76 (m, 2H, Ar-*H*), 7.20–7.17 (m, 2H, Ar-*H*), 3.90 (s, 2H, C*H*$_2$) ppm. ^{13}C NMR (125 MHz, DMSO-*d6*): δ 173.83 (*C*4-thiazolidinone ring), 164.82 (*C*2-thiazolidinone ring), 154.65 (H*C*=N), 149.82, 135.13, 133.58, 132.30, 131.84, 131.51, 129.13, 124.61, 122.53, 121.78 (Aromatic *C*), 124.58 (*C*F$_3$), 32.88 (*C*5-thiazolidinone ring) ppm. Mass (ES$^+$): 443.9059 (M)$^+$, 444.8917 (M+1)$^+$.

4.17. 4-(((4-Oxothiazolidin-2-ylidene)hydrazono)methyl)phenyl-2,4,6-triisopropylbenzenesulfonate (7m)

Yield: 76%; mp: 290–292 °C. ^{1}H NMR (500 MHz, DMSO-*d6*): δ 12.00 (s, 1H, N*H*), 8.39 (s, 1H, C*H*=N), 7.77–7.72 (m, 2H, Ar-*H*), 7.30 (s, 2H, Ar-*H*), 7.09–7.06 (m, 2H, Ar-*H*), 3.90 (s, 2H, C*H*$_2$), 3.82–3.89 (m, 3H, C*H*), 1.11 (d, *J* = 7.2 Hz, 6H, C*H*$_3$), 1.02 (d, *J* = 6.8 Hz, 12H, C*H*$_3$) ppm. ^{13}C NMR (125 MHz, DMSO-*d6*): δ 174.12 (*C*4-thiazolidinone ring), 164.84

(*C*2-thiazolidinone ring), 154.51 (H*C*=N), 150.36, 150.04, 133.18, 129.14, 128.67, 124.10, 122.58 (Aromatic *C*), 34.18 (*C*H), 33.00 (*C*H), 32.86 (*C*5-thiazolidinone ring), 24.56 (*C*H$_3$), 23.51 (*C*H$_3$) ppm. Mass (ES$^+$): 501.8402 (M)$^+$, 502.8513 (M+1)$^+$.

4.18. In vitro α-glucosidase inhibition assay

The α-glucosidase inhibitory activities of compounds (**7a-m**) were tested as per earlier described procedures [22,43]. In a 96-well plate, 60 μL of sample solution, prepared by dissolving test compounds in 5% DMSO and phosphate buffer [pH 6.8]), and 50 μL of 0.1 M phosphate buffer (pH 6.8) containing α-glucosidase solution (*Saccharomyces cerevisiae*) (0.2 U/ml) was incubated at 37 °C for 10 min. To this solution, 50 μL of 5 mM p-nitrophenyl-α-D-glucopyranoside (PNPG) solution in 0.1 M phosphate buffer (pH 6.8) was added and incubated at 37 °C for another 20 min. To stop the reaction, 40 μL of 0.8 M sodium carbonate was added to each well and the absorbance was recorded at 405 nm by microplate reader. For control, 60 μL of 5% DMSO was taken in place of the sample solution and acarbose was used as standard. The tests were performed in triplicate and percentage inhibition was calculated as follows:

$$\text{Inhibition}(\%) = \text{Absorbance of control} - \text{Absorbance of sample}/ \text{Absorbance of control} \times 100$$

The concentration of inhibitors corresponding to 50% of the α-glucosidase inhibition under the assay conditions was defined as the IC50 value

4.19. In vitro antioxidant activity (PFRAP assay)

The procedures for the determination of reducing potential of compounds (**7a-m**) were similarly followed as reported in our recent publications [22,43]. In a test tube, 2.5 ml of sample solution was mixed with 2.5 ml of phosphate buffer (0.2 M; pH 6.6) and 2.5 ml of 1% potassium ferricyanide solution. The mixture was incubated at 50 °C for 20 min, then rapidly cooled and mixed with 2.5 ml of 10% trichloroacetic acid. Then ferric chloride solution (0.5 ml, 0.1%) was added to an aliquot (2.5 ml) of the mixture diluted with 2.5 ml of distilled water and the solution was allowed to stand for 10 min. An aliquot of 5% DMSO (control) was treated similarly. Finally, absorbance was measured at 700 nm using UV spectrophotometer. The test samples were analyzed in triplicate and the data presented as mean ± standard error of the mean (SEM). The percent reducing power was calculated using the following formula:

$$\text{Reducing power}(\%) = A_{\text{test}} - A_{\text{control}}/A_{\text{test}} \times 100$$

4.20. In vivo oral disaccharide loading test

In vivo biological efficacy of the most potent compound (**7d**) has been evaluated by earlier reported methods [22,43]. Male albino mice were used to perform the sucrose loading test for **7d**. Animals (30–40 g) were fasted overnight and divided into different groups with five animals in each. The control group and reference group was orally administered with vehicle (0.5% carboxymethyl cellulose [CMC] solution) and standard drug acarbose (20 mg/kg body weight) dispersed in 0.5% CMC, respectively. Test groups were administered with homogenized suspension of **7d** (in 0.5% CMC and distilled water) at doses of 20 and 10 mg/kg body weight. After 20 min, the mice were given sucrose solution (2.5 g/kg body weight). Blood glucose level was estimated at 0 (before), 30, 60 and 120 min after sucrose solution loading using the Dr. Morepen GlucoOne (Morepen Laboratories Limited, Delhi, India) blood glucose monitoring system. The results were expressed as mean ± SEM. Area under blood glucose-time curve (AUC) over a period of 30 and 60 min after sucrose administration was calculated by GraphPad Prism version 5.01 (GraphPad, CA, USA). Statistical analysis was performed by two-way analysis of difference (ANOVA), followed by Bonferroni tests.

4.21. MTT assay

Cell viability was measured by standard colorimetric assay (MTT assay) following the procedure reported in our recent publication [22].

5. In silico studies

5.1. Homology model building and validation

The sequence of α-glucosidase was retrieved from UniProt (access code P53341) in FASTA format which was used for building of homology model through RaptorX server [50]. 3D crystal structure of oligo-1,6-glucosidase (PDB ID: 3A47, Gene ID: IMA1) of *Saccharomyces cerevisiae* was selected as best template for homology modeling. It has a high sequence similarity of 72.1 % and a p-value of 5.44e-20. Further, PROCHECK server (https://servicesn.mbi.ucla.edu/PROCHECK/) was used for obtaining Ramachandran plot. The 3D model structure and its quality has been validated by using QMEAN server and ProSA web server [51,52].

5.2. Molecular docking

The docking studies were performed using standard Glide (Glide, 2019) molecular docking protocol implemented in Maestro molecular modeling suite of Schrödinger, LLC,New York, NY, 2019. Modeled protein was treated using protein preparation wizard of Schrödinger suit where bond orders were assigned, hydrogens were added, bonds to metals were deleted, the formal charges on the metal and the neighbouring atoms were adjusted and finally water molecules were deleted. The protein structure was refined with the help of restrained minimization. The docking was performed using Glide extra precision mode (XP) [53–55]. The 3D crystal structure of oligo-1,6-glucosidase (isomaltase, PDB ID: 3A4A) of *Saccharomyces cerevisiae* was aligned on the homology model of alpha-glucosidase. Since, the binding site between of these two proteins is very similar, we used the co-ordinates of co-crystallised alpha-D-glucose from the isomaltase structure to define the docking site. The receptor grid was generated using the centroid of the co-crystallized alpha-D-glucose. During the docking studies, receptor was kept rigid and ligands were kept flexible. The final assessment was made on the basis of glide score (docking score).

The molecular simulation studies were carried out to calculate the binding free energies (ΔG_{bind}) of the synthesized hybrids with α-glucosidase. The Prime MM-GBSA panel was used to determine the ligand-binding energies and ligand strain energies for a set of ligands and α-glucosidase [56]. The Molecular Mechanics/Generalized Born Surface Area (MM-GBSA) procedure was used to calculate the binding free energy for all ligand- α-glucosidase complexes. The MM-GBSA method can be conceptually summarized as:

$$\Delta G_{bind} = G_{complex} - G_{receptor} - G_{ligand}$$

The ligand–receptor binding free energy change (ΔG_{bind}) was computed as the difference between the free energies of the complex ($G_{complex}$), the receptor ($G_{receptor}$), and the ligand (G_{ligand}).

5.3. ADME predictive studies

ADME predictive studies for synthesized compounds were performed following the procedures mentioned in our recent publication [22].

5.4. Molecular dynamic simulations

The molecular dynamic simulation studies for the docked complex of 7d and α-glucosidase over the period of 25ns were performed following procedures reported in our recent publication [22].

6. Conclusion

In the present investigation, sulfonate ester analogues of 2-(2-benzylidenehydrazono)thiazolidin-4-one have been synthesized and evaluated for their in vitro α-glucosidase inhibitory potential and antioxidant properties. The results of in vitro screening identified **7d** (IC$_{50}$: 42.80 ± 0.48 μM) as the most potent α-glucosidase inhibitor among the studied compounds. The rise of blood glucose level, after sucrose administration during in vivo studies, was more effectively controlled by **7d** (at a dose of 20 mg/kg of body weight) than acarbose. The results of MTT cytotoxicity assay established the safety profile of **7d**. Molecular docking studies identified the key binding interactions responsible for the snag fit of 7**d** within the binding cavity of enzyme. The confirmation stability of enzyme-**7d** complex over 25 ns long MD simulation further supported the higher enzyme inhibitory potential of **7d**. Additionally, appreciable antioxidant properties of compounds may supplement to reduce the oxidative stress mediated antidiabetic complications.

Declaration of Competing Interest

The authors declare no conflict of interest.

Acknowledgments

References

[1] D.R. Whiting, L. Guariguata, C. Weil, J. Shaw, IDF diabetes atlas: global estimates of the prevalence of diabetes for 2011 and 2030, Diabetes Res. Clin. Pract. 94 (2011) 311–321.

[2] M. Brownlee, The pathobiology of diabetic complications: a unifying mechanism, Diabetes 54 (2005) 1615–1625.

[3] American Diabetes Association, Diagnosis and classification of diabetes mellitus, Diabetes Care 32 (2009) S62–S567.

[4] J.M. Pappachan, C.J. Fernandez, E.C. Chacko, Diabesity and antidiabetic drugs, Mol. Asp. Med. 66 (2019) 3–12.

[5] Expert Committee on the Diagnosis and Classification of Diabetes Mellitus, Report of the expert committee on the diagnosis and classification of diabetes mellitus, Diabetes Care 20 (1997) 1183.

[6] D.L. Eizirik, T.M. Poulsen, A choice of death-the signal-transduction of immune-mediated beta-cell apoptosis, Diabetologia 44 (2001) 2115.

[7] M. Cnop, N. Welsh, J.C. Jonas, A. Jörns, S. Lenzen, D.L. Eizirik, Mechanisms of pancreatic β-cell death in type 1 and type 2 diabetes, Diabetes Care 54 (2005) S97.

[8] A.J. Scheen, Is there a role for α-glucosidase inhibitors in the prevention of type 2 diabetes mellitus? Drugs 63 (2003) 933–951.

[9] M. Saeedi, M.M. Khanaposhtani, M.S. Asgari, N. Eghbalnejad, S. Imanparast, M.A. Faramarzi, B. Larijani, M. Mahdavi, T. Akbarzadeh, Design, synthesis, in vitro, and in silico studies of novel diaryl imidazole-1,2,3-triazole hybrids as potent α-glucosidase inhibitors, Bioorg. Med. Chem. 27 (2019) 115148.

[10] M. Saeedi, A. Hadjiakhondi, S.M. Nabavi, A. Manayi, Heterocyclic compounds: effective α-amylase and α-glucosidase inhibitors, Curr. Top. Med. Chem. 17 (2017) 428–440.

[11] K.R. Raju, A.R.G. Prasad, B.S. Kumar, L.K. Ravindranath, Synthesis and antimicrobial activity of novel heterocycles containing thiazolidinone and 1,3,4-oxadiazole moieties, J. Clin. Anal. Med. 7 (2016) 14–17.

[12] S. Grasso, A. Chimirri, P. Monforte, G. Fenech, M. Zappala, A.M. Monforte, Pharmacol. Sci. 43 (1988) 851.

[13] M.V. Diurno, O. Mazzoni, E. Piscopo, A. Calignano, F. Giordano, A. Bolognese, Synthesis and antihistaminic activity of some thiazolidin-4-ones, J. Med. Chem. 35 (1992) 2910–2912.

[14] G.C. Look, J.R. Schullek, C.P. Holmes, J.P. Chinn, E.M. Gordon, M.A. Gallop, The identification of cyclooxygenase-1 inhibitors from 4-thiazolidinone combinatorial libraries, Bioorg. Med. Chem. 6 (1996) 707–712.

[15] M. Faizia, R. Jahania, S.A. Ebadib, S.A. Tabatabaic, E. Rezaeec, M. Lotfalieic, M. Aminid, A. Almasirad, Novel 4-thiazolidinone derivatives as agonists of benzodiazepine receptors: design, synthesis and pharmacological evaluation, EX-CLI J. 16 (2017) 52–62.

[16] K. Babaoglu, M.A. Page, V.C. Jones, M.R. McNeil, C. Dong, J.H. Naismith, R.E. Lee, Novel inhibitors of an emerging target in mycobacterium tuberculosis; substituted thiazolidinones as inhibitors of dtdp-rhamnose synthesis, Bioorg. Med. Chem. Lett. 13 (2003) 3227–3230.

[17] V. Ravichandran, A. Jain, K.S. Kumar, H. Rajak, R.K. Agrawal, Design, synthesis, and evaluation of thiazolidinone derivatives as antimicrobial and anti-viral agents, Chem. Biol. Drug Des. 78 (2011) 464–470.

[18] R. Bhutani, D.P. Pathak, G. Kapoor, A. Husain, M. AzharIqbal, Novel hybrids of benzothiazole-1,3,4-oxadiazole-4-thiazolidinone: synthesis, in silico ADME study, molecular docking and in vivo anti-diabetic assessment, Bioorg. Chem. 83 (2019) 6–19.

[19] S.K. Manjal, R. Kaur, R. Bhatia, K. Kumar, V. Singh, R. Shankar, R. Kaur, R.K. Rawal, Synthetic and medicinal perspective of thiazolidinones: a review, Bioorg. Chem. 75 (2017) 406–423.

[20] A. Verma, S.K. Saraf, 4-Thiazolidinone-A biologically active scaffold, Eur. J. Med. Chem. 43 (2008) 897–905.

[21] F. Rahim, M. Taha, H. Ullah, A. Wadood, M. Selvaraj, A. Rab, M. Sajid, S.A.A. Shah, N. Uddin, M. Gollapalli, Synthesis of new arylhydrazide bearing Schiff bases/thiazolidinone:α-amylase, urease activities and their molecular docking studies, Bioorg. Chem. 91 (2019) 103112.

[22] R. Kaur, R. Kumar, N. Dogra, A. Kumar, A.K. Yadav, M. Kumar, Synthesis and studies of thiazolidinedione-isatin hybrids as α-glucosidase inhibitors for management of diabetes, Future Med. Chem. 13 (2021) 457–485.

[23] B.P. Bandgar, S.V. Bettigeri, J. Phopase, Unsymmetrical Diaryl Sulfones through palladium-catalyzed coupling of aryl boronic acids and arylsulfonyl chlorides, Org. Lett. 6 (2004) 2105–2108.

[24] S.H. Gund, R.S. Shelkar, J.M. Nagarkar, Copper catalyzed synthesis of unsymmetrical diaryl sulfones from an arenediazonium salt and sodium p-toluenesulfinate, RSC Adv. 5 (2015) 62926–62930.

[25] M.K. Mahapatra, R. Kumar, M. Kumar, Synthesis, biological evaluation and in silico studies of 5-(3-methoxybenzylidene)thiazolidine-2,4-dione analogues as PTP1B inhibitors, Bioorg. Chem. 71 (2017) 1–9.

[26] S. Wang, J. Yan, X. Wang, Z. Yang, F. Lin, T. Zhang, Synthesis and evaluation of the α-glucosidase inhibitory activity of 3-[4-(phenylsulfonamido)benzoyl]-2H-1-benzopyran-2-one derivatives, Eur. J. Med. Chem. 45 (2010) 1250–1255.

[27] M. Gollapalli, M. Taha, H. Ullah, M. Nawaz, L.M.R. AlMuqarrabun, F. Rahim, F. Qureshi, Ashik Mosaddik, N. Ahmat, K.M. Khan, Synthesis of bis-indolylmethane sulfonohydrazides derivatives as potent α-glucosidase inhibitors, Bioorg. Chem. 80 (2018) 112–120.

[28] X. Bian, Q. Wang, C. Ke, G. Zhao, Y. Li, A new series of N2-substituted-5-(p-toluenesulfonylamino)phthalimide analogues as α-glucosidase inhibitors, Bioorg. Med. Chem. Lett. 23 (2013) 2022–2026.

[29] S. Riaz, I.U. Khan, M. Bajda, M. Ashraf, Qurat-Ul-Ain, A. Shaukat, T.U. Rehman, S. Mutahir, S. Hussain, G. Mustafa, M. Yar, Pyridine sulfonamide as a small key organic molecule for the potential treatment of type-II diabetes mellitus and Alzheimer's disease: in vitro studies against yeast α-glucosidase, acetylcholinesterase and butyrylcholinesterase, Bioorg. Chem. 63 (2015) 64–71.

[30] M.I. Osella, M.O. Salazar, M.D. Gamarra, D.M. Moreno, F. Lambertucci, D.E. Frances, R.L.E. Furlan, Arylsulfonyl histamine derivatives as powerful and selective α-glucosidase inhibitors, RSC Med. Chem. 11 (2020) 518–527.

[31] Q.U.N. Tariq, S. Malik, A. Khan, M.M. Naseer, S.U. Khan, A. Ashraf, M. Ashraf, M. Rafiq, K. Mahmood, M.N. Tahir, Z. Shafiq, Xanthenone-based hydrazones as potent α-glucosidase inhibitors: synthesis, solid state self-assembly and *in silico* studies, Bioorg. Chem. 84 (2019) 372–383.

[32] S. Imran, M. Taha, N.H. Ismail, S.M. Kashif, F. Rahim, W. Jamil, M. Hariono, M. Yusuf, H. Wahab, Synthesis of novel flavone hydrazones: *in-vitro* evaluation of α-glucosidase inhibition, QSAR analysis and docking studies, Eur. J. Med. Chem. 105 (2015) 156–170.

[33] G. Wang, M. Chen, J. Wang, Y. Peng, L. Li, Z. Xie, B. Deng, S. Chen, W. Li, Synthesis, biological evaluation and molecular docking studies of chromone hydrazone derivatives as α-glucosidase inhibitors, Bioorg. Med. Chem. Lett. 27 (2017) 2957–2961.

[34] M. Taha, S.A.A. Shah, M. Afifi, S. Imran, S. Sultan, F. Rahim, K.M. Khan, Synthesis, α-glucosidase inhibition and molecular docking study of coumarin based derivatives, Bioorg. Chem. 77 (2018) 586–592.

[35] M. Taha, N.H. Ismail, S. Imran, M.Q.B. Rokei, S.M. Saad, K.M. Khan, Synthesis of new oxadiazole derivatives as α-glucosidase inhibitors, Bioorg. Med. Chem. 23 (2015) 4155–4162.

[36] M. Taha, N.H. Ismail, S. Imran, A. Wadood, M. Ali, F. Rahim, A.A. Khan, M. Riaz, Novel thiosemicarbazide-oxadiazole hybrids as unprecedented inhibitors of yeast α-glucosidase and *in silico* binding analysis, RSC Adv. 6 (2016) 33733–33742.

[37] T.H. Duong, A.P. Devi, N.M.A. Tran, H.V.T. Phan, N.V. Huynh, J. Sichaem, H.D. Tran, M. Alam, T.P. Nguyen, H.H. Nguyen, W. Chavasiri, T.C. Nguyen, Synthesis, α-glucosidase inhibition, and molecular docking studies of novel N-substituted hydrazide derivatives of atranorin as antidiabetic agents, Bioorg. Med. Chem. Lett. 30 (2020) 127359.

[38] F. Ali, K.M. Khan, U. Salar, M. Taha, N.H. Ismail, A. Wadood, M. Riaz, S. Perveen, Hydrazinyl arylthiazole based pyridine scaffolds: synthesis, structural characterization, *in vitro* α-glucosidase inhibitory activity, and *in silico* studies, Eur. J. Med. Chem. 138 (2017) 255–272.

[39] A.N. Kawde, M. Taha, R.S. Alansari, N.B. Almandil, E.H. Anouar, N. Uddin, F. Rahim, S. Chigurupati, M. Nawaz, S. Hayat, M. Ibrahim, P.K. Elakurthy, V. Vijayan, M. Morsy, H. Ibrahim, N. Baig, K.M. Khan, Exploring efficacy of indole-based dual inhibitors for α-glucosidase and α-amylase enzymes: *in silico*, biochemical and kinetic studies, Int. J. Biol. Macromol. 154 (2020) 217–232.

[40] M. Ozil, M. Emirik, A. Belduz, S. Ulker, Molecular docking studies and synthesis of novel bisbenzimidazole derivatives as inhibitors of α-glucosidase, Bioorg. Med. Chem. 24 (2016) 5103–5114.

[41] F. Rahim, K. Zaman, M. Taha, H. Ullah, M. Ghufran, A. Wadood, W. Rehman, N. Uddin, S.A.A. Shah, M. Sajid, F. Nawaz, K.M. Khan, Synthesis, *in vitro* alpha-glucosidase inhibitory potential of benzimidazole bearing bis-Schiff bases and their molecular docking study, Bioorg. Chem. 94 (2020) 103394.

[42] A. Aispuro-Pérez, J. López-Ávalos, F. García-Páez, J. Montes-Avila, L.A. Picos-Corrales, A.N. Ochoa-Terán, P. Bastidas, S. Montaño, L. Calderón-Zamora, U. Osuna–Martínez, J.I. Sarmiento-Sánchez, Synthesis and molecular docking studies of imines as α-glucosidase and α-amylase inhibitors, Bioorg. Chem. 94 (2020) 103491.

[43] R. Kaur, K. Palta, M. Kumar, Hybrids of isatin-pyrazole as potential α-glucosidase inhibitors: synthesis, biological evaluations and molecular docking studies, ChemistrySelect 4 (2019) 13219–13227.

[44] A. Ceriello, R. Testa, Antioxidant anti-inflammatory treatment in type 2 diabetes, Diabetes Care 32 (2) (2009) S232–S236 suppl.

[45] G. Oboh, O.B. Ogunsuyi, M.D. Ogunbadejo, S.A. Adefegha, Influence of gallic acid on α-amylase and α-glucosidase inhibitory properties of acarbose, J. Food Drug Anal. 24 (2016) 627–634.

[46] M. Källberg, H. Wang, S. Wang, J. Peng, Z. Wang, H. Lu, J. Xu, Template-based protein structure modeling using the RaptorX web server, Nat. Protoc. 7 (2012) 1511–1522.

[47] QikProp, V5.2., Schrödinger, Suite 2019, LLC, New York, NY, 2012.

[48] H.J. Ahr, M. Boberg, H.P. Krause, W. Maul, F.O. Müller, H.J. Ploschke, H. Weber, C. Wünsche, Pharmacokinetics of acarbose. Part I: absorption, concentration in plasma, metabolism and excretion after single administration of [14C]acarbose to rats, dogs and man, Arzneimittelforschung 39 (1989) 1254–1260.

[49] F. Rahim, K. Zaman, H. Ullah, M. Taha, A. Wadood, M.T. Javed, W. Rehman, M. Ashraf, R. Uddin, I. Uddin, H. Asghar, A.A. Khan, K.M. Khan, Synthesis of 4-thiazolidinone analogs as potent *in vitro* anti-urease agents, Bioorg. Chem. 63 (2015) 123–131.

[50] M. Källberg, H. Wang, S. Wang, J. Peng, Z. Wang, H. Lu, J. Xu, Template-based protein structure modeling using the RaptorX web server, Nat. Protoc. 7 (2012) 1511–1522.

[51] P. Benkert, S.C.E. Tosatto, D. Schomburg, QMEAN: a comprehensive scoring function for model quality assessment, Proteins 71 (2008) 261–277.

[52] M. Wiederstein, M.J. Sippl, ProSA-web: interactive web service for the recognition of errors in three-dimensional structures of proteins, Nucleic Acids Res. 35 (2007) W407–W410.

[53] R.A. Friesner, J.L. Banks, R.B. Murphy, T.A. Halgren, J.J. Klicic, D.T. Mainz, M.P. Repasky, E.H. Knoll, M. Shelley, J.K. Perry, D.E. Shaw, P. Francis, P.S. Shenkin, Glide: a new approach for rapid, accurate docking and scoring. 1. Method and assessment of docking accuracy, J. Med. Chem. 47 (2004) 1739–1749.

[54] T.A. Halgren, R.B. Murphy, R.A. Friesner, H.S. Beard, L.L. Frye, W.T. Pollard, J.L. Banks, Glide: a new approach for rapid, accurate docking and scoring. 2. Enrichment factors in database screening, J. Med. Chem. 47 (2004) 1750–1759.

[55] R.A. Friesner, R.B. Murphy, M.P. Repasky, L.L. Frye, J.R. Greenwood, T.A. Halgren, P.C. Sanschagrin, D.T. Mainz, Extra precision glide: docking and scoring incorporating a model of hydrophobic enclosure for protein-ligand complexes, J. Med. Chem. 49 (2006) 6177–6196.

[56] Y. Yang, Y. Shen, H. Liu, X. Yao, Molecular dynamics simulation and free energy calculation studies of the binding mechanism of allosteric inhibitors with p38a MAP kinase, J. Chem. Inf. Model. 51 (2011) 3235–3246.